AUTHORS' ACCEPTED MANUSCRIPT

INTERNATIONAL JOURNAL OF MECHANICAL SCIENCES

Intrinsic non-flat-foldability of two-tile DDC surfaces composed of glide-reflected irregular quadrilaterals

Pooya Sareh[a,*], Yao Chen[b,*]

[a] Creative Design Engineering Lab (Cdel), School of Engineering, University of Liverpool, Liverpool, The Quadrangle, Brownlow Hill, L69 3GH, United Kingdom
[b] Key Laboratory of Concrete and Prestressed Concrete Structures of Ministry of Education, and National Prestress Engineering Research Center, Southeast University, Nanjing 211189, China

A B S T R A C T

Functional origami tessellations have certain geometric or physical properties - such as flat-foldability and rigid-foldability - which make them of particular interest for a broad range of applications in science, engineering, and architecture. While some simple variations of certain functional origami tessellations can be designed trivially, a systematic symmetry-reduction scheme is proved to be productive for the computational generation of more complex, non-trivial variations. Such a scheme has been previously applied to the developable double corrugation (DDC) surface, widely known as the Miura-ori, resulting in the development of novel crystalline derivatives, the symmetry groups of which are subgroups of the parent pattern. Computational algorithms can search for and find flat-foldable solutions for a large number of derivatives of the DDC surface, but fail to find solutions for all of them. In this paper, we exploit the symmetry reduction scheme along with classical plane geometry to analytically demonstrate why some crystallographic derivatives of this pattern do not exist. To this end, by applying the local flat-foldability condition at the vertices of different orbits associated with each tessellation, we show that such patterns are never flat-foldable, regardless of the geometric specifications of their constituting quadrilateral facets. In particular, we prove that two-tile DDC surfaces composed of glide-reflected irregular quadrilaterals are intrinsically non-flat-foldable, resulted from geometric incompatibilities between the properties of certain unit cells and the local flat-foldability condition.

1. Introduction

Origami – the traditional art of paper folding – has inspired countless practical applications over the past few decades. In particular, some origami tessellations have attracted the enormous interest of science and engineering communities, as a result of their design versatility and favourable mechanical properties such as limited degrees of freedom [1–4], stiffness-tunability [5–10], flat-foldability [11,12], and rigid-foldability [13–16] (stiffness-tunability is the condition of having tunable structural stiffness; flat-foldability means that an originally planar thin sheet can be folded to a second 'flat' configuration; rigid-foldability implies that the facets of the origami structure remain flat during folding/unfolding).

One of the most noted and widely-used origami tessellations in science, engineering, and architecture is the developable double corrugation (DDC) surface, popularly known as the Miura-ori. As can be seen from Fig. 1a, the crease lines of this pattern form parallelograms (more precisely, a single parallelogram repeated in two directions) which tessellate the plane. Variations of the DDC surface have also found numerous applications. As a result, developing new functional variations could potentially expand the range of applications for such a fold pattern in various fields. To this end, the next section presents the mathematical concepts and definitions that are necessary to explore and design new variations for this tessellation.

2. Theoretical background

From a mathematical standpoint, symmetry is an intrinsic property of every repetitive structure. On a broader level, symmetry analysis is an insightful approach to the design and analysis of engineering structures of different types such as truss structures [17–28], tensegrities [29–32], and layered space grids [33,34]. Therefore, to analyse the composition and design of a given tessellation, one needs to investigate symmetry elements associated with that tessellation.

Transformational geometry is the branch of mathematics studying geometric transformations, which underlie the modern understanding of symmetry [35]. A *transformation* τ on a set S is a function from S to S that is both one-to-one and onto, i.e. it is a one-to-one correspondence from S to itself [36,37]. An *isometry* is a *distance-preserving* transformation. Mathematically speaking, a transformation $\tau\colon \mathbb{R}^2 \to \mathbb{R}^2$ is an isometry of the plane $\mathbb{R}^2$ if for any two points P and Q of $\mathbb{R}^2$, the Euclidean distance between P and Q remains invariant, i.e., $|\tau(P) - \tau(Q)| = |P - Q|$ [38,39]. In fact, an isometry is a special case of a *similarity* (similarities are *angle-preserving* transformations which characterise Euclidean geometry) [40,41].

With the above concepts and definitions in mind, one can observe that every infinite, two-dimensional tessellation is composed of a design motif transformed by a group of isometries to cover the plane without any gap or overlap. In general, the isometries of the two-dimensional

* Corresponding authors.
E-mail addresses: pooya.sareh@liverpool.ac.uk, pooya.sareh@gmail.com (P. Sareh), chenyao@seu.edu.cn (Y. Chen).

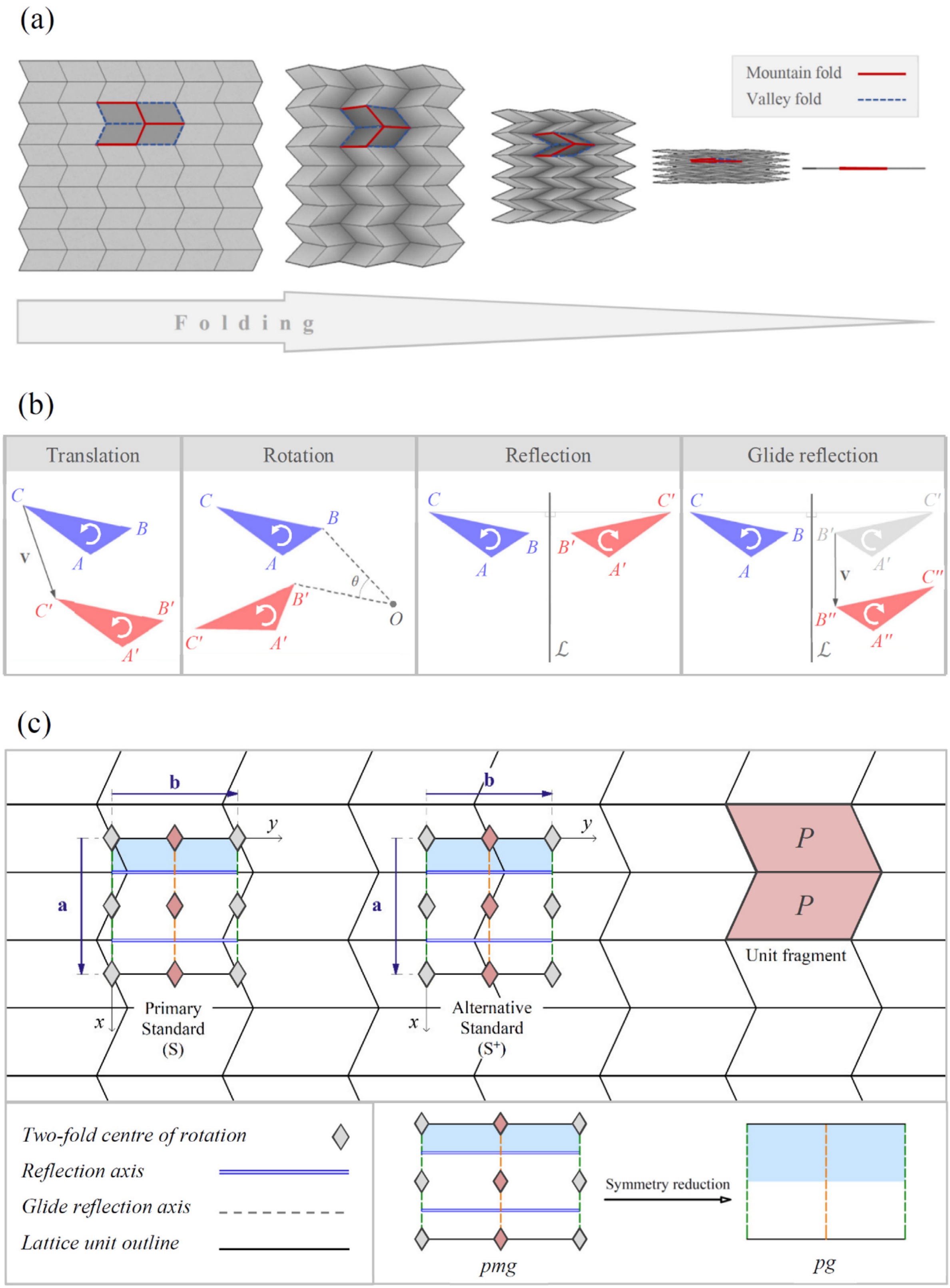

Fig. 1. (a) Folding sequence of a typical developable double corrugation (DDC) surface or the Miura-ori; a 2×2 unit of this pattern is illustrated along with the mountain-valley assignment of crease lines (the thickness of the surface is assumed to be negligible). (b) Different types of non-trivial isometries of the plane. (c) Two standard choices for the smallest *pmg* unit cell for the Miura fold pattern (top), and the symmetry reduction of a *pmg* unit cell to a *pg* unit cell by removing the centres of rotation and axes of reflection (bottom right). The blue shaded area shows the fundamental region of the pattern. Different colours for a symmetry element represent different classes of that element in the pattern. The directions in which horizontal lines and zigzag polylines travel are respectively called the longitudinal and transverse directions of the pattern, represented by the y- and x-axes, respectively. The unit fragment of the pattern, composed of two adjacent parallelograms (denoted by P), is illustrated on the top right.

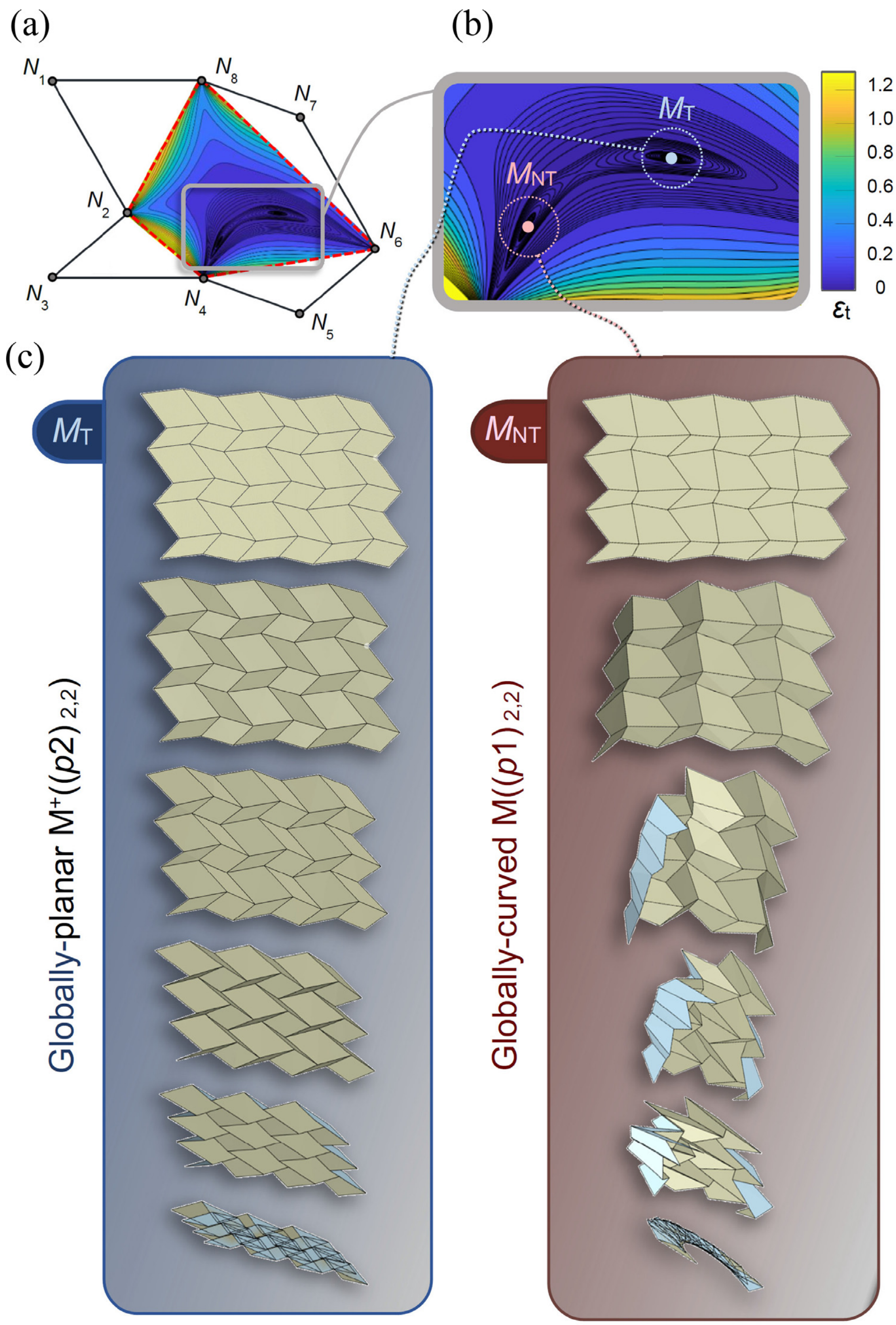

Fig. 2. (a) The core quadrilateral (depicted by red dashed lines) and the distribution of the total flat-foldability error for a typical octagonal unit fragment associated with the two plane symmetry groups $p1$ and $p2$. (b) Close-up of error distribution showing two local minima. (c) Two flat-foldable solutions corresponding to the two minima given in part b.

plane include the identity, rotations, reflections, and glide reflections, as illustrated in Fig. 1b.

According to the classification of two-dimensional symmetry groups [42,43], the symmetry of the Miura fold pattern is 22* in the Orbifold notation [44], $[(\infty,2)^+,\infty]$ or $[\infty,(2,\infty)^+]$ in the Coxeter notation (see, e.g., [45] or [46]), or *pmg* in the International Union of Crystallography (IUCr) notation [47]. In this paper, the Miura fold pattern is denoted by M. According to [48], there are two choices for the smallest unit cell of a given Miura crease pattern that both match the standard *pmg* unit cell used in the IUCr tables [47], as illustrated in Fig. 1c: the 'primary standard' choice S, and the 'alternative standard' choice S^+. It has been shown [48] that these two initial choices produce the same descendants for some symmetric variations, whereas they generate different results for some others. Hereafter in this study, those descendants of the Miura-ori which can only be generated based on S^+ are denoted by M^+.

A 'unit fragment' of a tessellating mesh is defined as a minimal collection of adjacent facets which can generate the entire tessellation using its respective translation vectors [49]. As illustrated on the top right of Fig. 1c, the unit fragment of a Miura fold pattern is composed of two adjacent parallelograms (denoted by *P*) which share a fold line on the horizontal lines of the pattern.

Designers and researchers in various fields have proposed a range of variations for the Miura-ori [11,50–52]. A framework for the generalisation of this origami tessellation is developed and presented in [49].

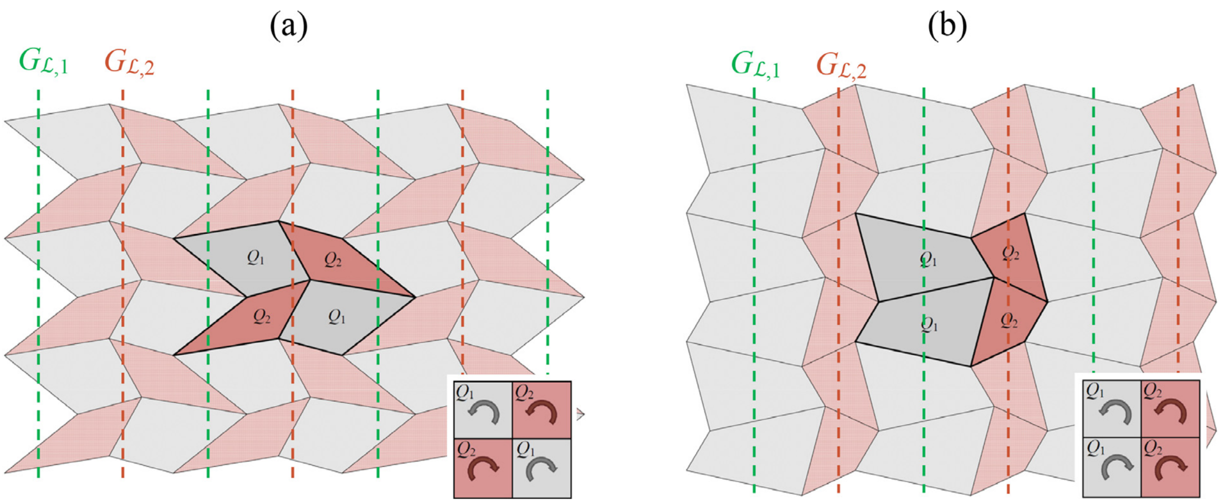

Fig. 3. **(a)** An M($pg_{2,2}$) tessellation. **(b)** An M$^+$($pg_{2,2}$) tessellation. Different colours for glide reflection axes (dashed lines) represent different classes of the symmetry element in the patterns (i.e., $G_{\mathcal{L},1}$ and $G_{\mathcal{L},2}$). The orientation of each quadrilateral is reserved because glide reflection is an indirect (or sense-reversing) isometry, as can be seen from the 2 × 2 module of representative squares on the bottom right corner of each tessellation.

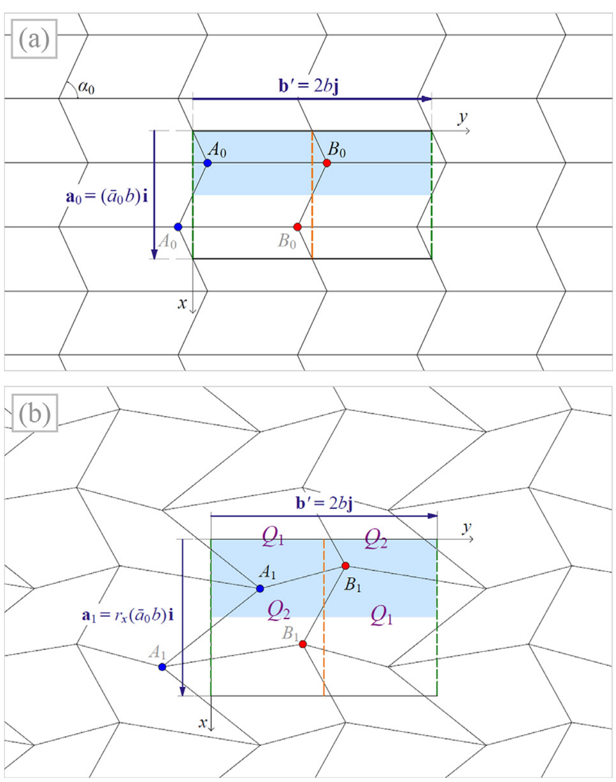

Fig. 4. An M($pg_{2,2}$) tessellation. (a) State 0: a given Miura fold pattern. (b) State 1: a symmetrically perturbed state using all degrees of freedom.

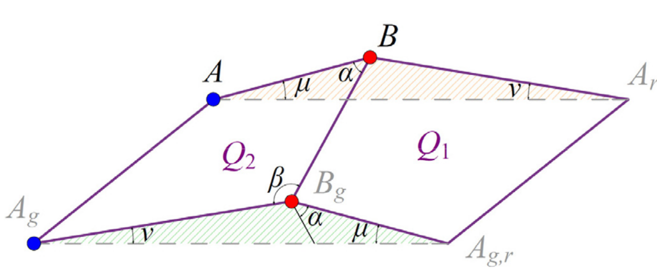

Fig. 5. A pair of consecutive quadrilaterals in the y-direction from State 1 of the previous figure.

According to this framework, a repetitive convex quadrilateral mesh designed by displacing the nodes of a conventional DDC crease pattern is called $G_{i,j}$, where G is the name of its maximal plane symmetry group, and i and j are the number of quadrilaterals in the x- and y-directions, respectively, within the unit cell of the pattern. The y-direction is the direction of the parallel fold lines in the Miura fold pattern before applying variations. Variations of the DDC crease pattern which can only be designed based on the alternative standard unit cell S$^+$ (shown in Fig. 1c) are denoted by $G^+{}_{i,j}$. This framework was applied to the design of a range of isomorphic [53] and non-isomorphic [54] symmetric descendants of the Miura-ori. It should be noted that according to this framework the mountain-valley assignment of the crease lines does not affect the symmetry of a tessellation.

While some simple flat-foldable variations of the DDC crease pattern can be designed trivially, some others require careful crystallographic considerations and geometric calculations. A systematic symmetry-reduction scheme is proved to be productive for the generation of some more complex, non-trivial derivatives. The design of some of these non-trivial variations involves considerable geometric complexities which require effective computational strategies and algorithms.

To explore the existence and design of such diverse solutions, here we present a computational framework which evaluates the flat-foldability of various degree-4 tessellations. Consider a central point $M = [X_0\ Y_0]$ and four surrounding points $N_1 = [X_1\ Y_1]$, $N_2 = [X_2\ Y_2]$, $N_3 = [X_3\ Y_3]$, and $N_4 = [X_4\ Y_4]$ in the Cartesian coordinate system. Let us define a 4 × 2 matrix $\mathbf{N} = [\ N_1 \quad N_2 \quad N_3 \quad N_4\ ]^T$ containing all the surrounding points. The line segment connecting each point N_i ($i = 1$, 2, …, 5; and $N_5 \equiv N_1$) to node M is denoted by l_i and the angle between any two successive line segments l_i and l_{i+1} in the counter-clockwise direction around M is named $\alpha_{i(i+1)}$ (note that $\alpha_{45} = \alpha_{41}$ as $N_5 \equiv N_1$). We define the *local flat-foldability error function*, ε, as a function of $\mathbf{N}$ and M as follows

$$\varepsilon(\mathbf{N}, M) = \left(\pi - \left\{\alpha_{12}(\mathbf{N}, M) + \alpha_{34}(\mathbf{N}, M)\right\}\right)^2 \tag{1}$$

To show examples for trivial and non-trivial solutions, let us consider the boundaries of a general 2 × 2 module (i.e., an 'octagonal unit fragment' [12]) as illustrated in Fig. 2a. Denoting the errors for nodes N_4, N_5, N_6 and M (the unknown central vertex) as ε_4, ε_5, ε_6, and ε_m, respectively, the *total flat-foldability error* ε_t of the tessellation is defined as

$$\varepsilon_t = \sqrt{\varepsilon_4^2 + \varepsilon_5^2 + \varepsilon_6^2 + \varepsilon_m^2} \tag{2}$$

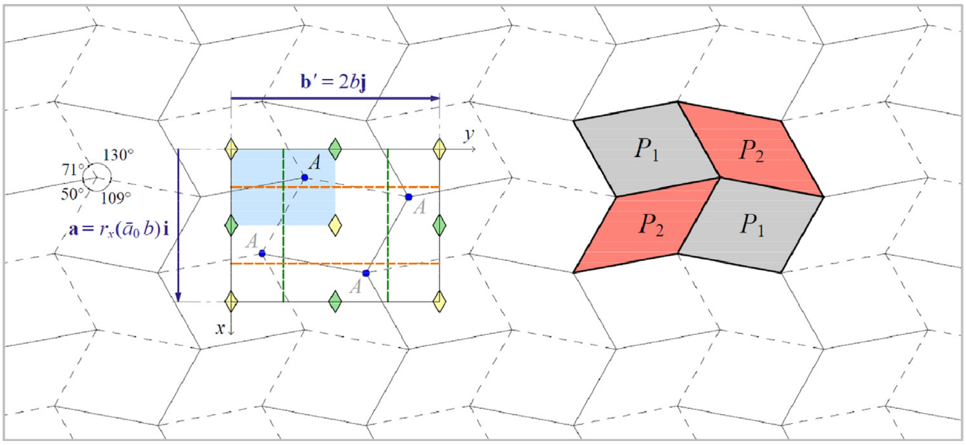

Fig. 6. An example of a $pgg^{+}_{2,2}$ variation of the Miura-ori, consisting of two different starting parallelograms P_1 and P_2. Solid and dashed lines represent mountain and valley folds, respectively. The blue shaded area shows the fundamental region of the pattern. Different colours for a symmetry element represent different classes of that element in the pattern [54].

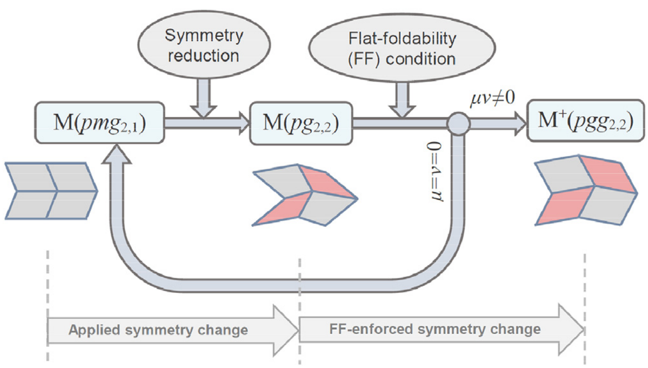

Fig. 7. Design generation process of the $pg_{2,2}$ derivative of the DDC surface.

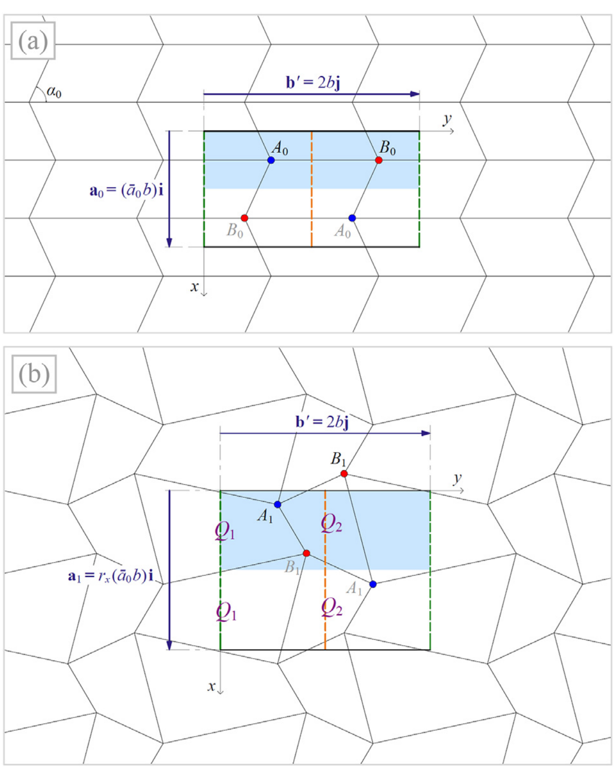

Fig. 8. An M$^+$($pg_{2,2}$) tessellation. **(a)** State 0: a given Miura fold pattern. **(b)** State 1: a symmetrically perturbed state using all degrees of freedom.

We use this definition for the total flat-foldability error as an objective function to be minimized. Fig. 2a shows the 'core quadrilateral' [12] and the distribution of the total flat-foldability error for a typical octagonal unit fragment associated with the two plane symmetry groups with parallelogram unit cells, i.e. $p1$ and $p2$. A close-up of the error distribution in the vicinity of the two local minima of the error function is shown in Fig. 2b. As can be seen from Fig. 2c, one of these two minima generates a trivial solution, M_T, for which the internal fold lines are piece-wise parallel to the borders of the octagonal unit fragment; this produces an M$^+$($(p2)_{2,2}$) derivative of the DDC surface, which is globally-planar. On the other hand, the other local minimum generates a non-trivial solution, M_{NT}, which produces an M($(p1)_{2,2}$) derivative of the DDC surface, which is globally-curved.

In contrast to the above example, there are some cases in which whilst the geometry is relatively simple and the number of unknowns is only a few, we can observe that no computational algorithm would generate any valid flat-foldable solution. The non-existence of such functional variations is generally a result of clashes between crystallographic restrictions and the local flat-foldability condition. The next section deals with two specific derivatives of the Miura-ori which are of this type.

3. Design and analysis of *pg* derivatives of the DDC surface

In transformational geometry, a reflection in line $\mathcal{L}$, denoted by $R_{\mathcal{L}}$, followed by a translation T parallel to $\mathcal{L}$, denoted by $T_{\mathcal{L}}$(alternatively, the translation followed by the reflection), is called a glide reflection, represented by $G_{\mathcal{L}|T}$ in this paper. In other words

$$G_{\mathcal{L}|T}(P) = \left[R_{\mathcal{L}} \circ T_{\mathcal{L}}\right](P) = \left[T_{\mathcal{L}} \circ R_{\mathcal{L}}\right](P), \tag{3}$$

where P is a point on the plane and ○ denotes the composition of functions. In the x-y Cartesian coordinate system, with the assumptions that $\mathcal{L}$ passes through O and makes an angle φ with the positive x-axis (i.e., $\mathcal{L}: \; y = x\tan\varphi$), the transformed coordinates of point P under $G_{\mathcal{L}|T}$, denoted by P', can be expressed as

$$P' = \begin{bmatrix} x' \\ y' \end{bmatrix} = G_{\mathcal{L}|T}(P) = \begin{bmatrix} \cos 2\varphi & \sin 2\varphi \\ \sin 2\varphi & -\cos 2\varphi \end{bmatrix} \begin{bmatrix} x \\ y \end{bmatrix} + \begin{bmatrix} T_x \\ T_y \end{bmatrix}. \tag{4}$$

Amongst the seventeen plane symmetry groups, the group pg is the only group that contains glide reflections only, without any rotations or reflections. Depending on the choice of the standard unit cell (see Fig. 1c), there are two minimal pg derivatives of the DDC crease pattern in the longitudinal direction. These two pg derivatives, represented by M($pg_{2,2}$) and M$^+$($pg_{2,2}$), are depicted in parts a and b of Fig. 3, respectively. As can be seen from the figure, both patterns are composed of two irregular quadrilaterals, with a difference in their compositions, as conceptualised by a 2 × 2 module of representative squares on the bottom right corner

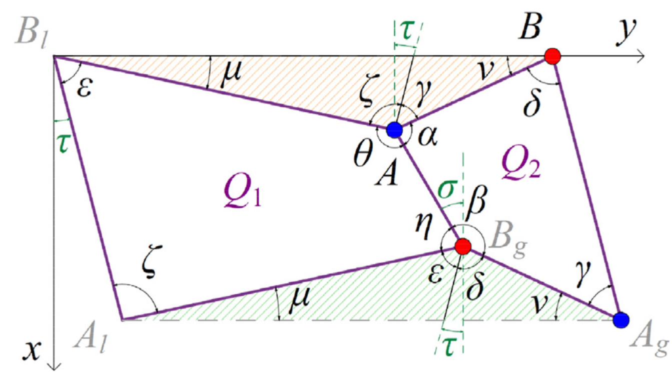

Fig. 9. A pair of consecutive quadrilaterals in the y-direction from State 1 of the previous figure.

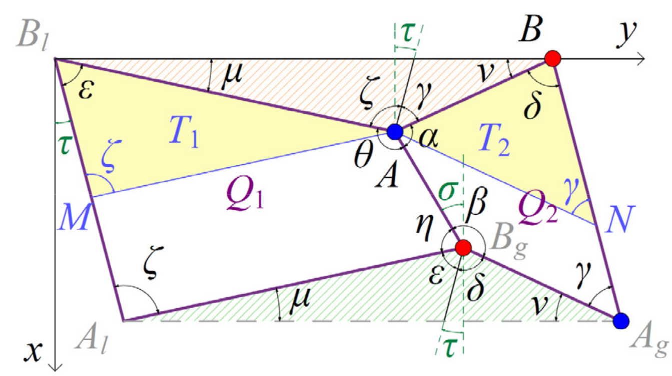

Fig. 10. Two line segments AM and AN, parallel to B_gA_l and B_gA_g respectively, are added to the previous figure to form triangles T_1 and T_2.

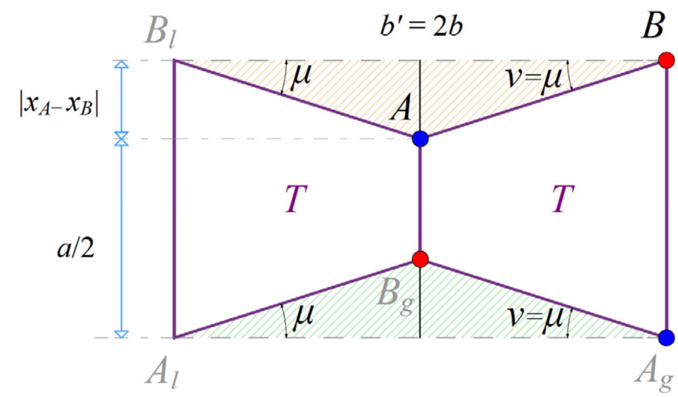

Fig. 11. Q_1 and Q_2 are two congruent isosceles trapezoids, T, with a base equal to $\frac{a}{2} + |x_A - x_B|$ and a height (altitude) equal to b.

of each tessellation. This section proves the impossibility of flat-folding such tessellations.

3.1. *The* M($pg_{2,2}$) *tessellation*

Theorem 3.1. *An* M($pg_{2,2}$) *tessellation is never flat-foldable.*

Proof. An M($pg_{2,2}$) unit cell is depicted in its original configuration, State 0, in Fig. 4a. There are two distinct orbits of nodes associated with the unit cell, shown as A_0 and B_0. Since we are dealing with a pg group, we have a degree of freedom for the aspect ratio of the unit cell (r_x is the scale factor in the x-direction). We are allowed to move nodes A_0 and B_0 in the x- or y-directions; however, we know that pg cannot fix the unit cell in the x-direction. Therefore, for a fixed set of $\bar{a}$, y_A, y_B, there is a single degree of freedom for $x_A - x_B$. (It should be noted that changing the sign of $x_A - x_B$, while keeping the other degrees of freedom fixed, makes the pattern reflected with respect to the x-axis). In Fig. 4b, we have perturbed the pattern using all the degrees of freedom that we introduced earlier to obtain a new configuration, State 1.

With the purpose of examining the application of the flat-foldability condition to the pattern at nodes A and B, we have illustrated a pair of consecutive quadrilaterals in the y-direction, from State (2) of the previous figure, in Fig. 5. Nodes with index r represent the equivalent nodes on the right of respective nodes. For clarity, as we are dealing with a geometry problem, we ignore the naming scheme for symmetrically equivalent nodes associated with a unit cell. We have renamed the grey nodes A and B (see Fig. 5) as A_g and B_g, where g stands for glide-reflected.

Line segments AB and $B_gA_{g,r}$ have the same length, and the same acute angle (the absolute value of the angle is considered) with respect to the y-axis, μ, as a result of the glide-reflection transformation. There is a similar relationship between line segments BA_r and B_gA_g, which intersect the y-axis at an angle axis ν (we assume that $\mu \neq 0$ and $\nu \neq 0$). Applying the local flat-foldability condition at node B_g, we obtain

$$\alpha + \beta = \pi, \tag{5}$$

which implies that

$$AB \parallel A_gB_g. \tag{6}$$

In other words

$$\mu = \nu. \tag{7}$$

Therefore, $T_1 = AA_rB$ and $T_2 = A_gA_{g,r}\, B_g$ are two congruent isosceles triangles. As a result

$$AB = A_gB_g. \tag{8}$$

From Eqs. (6) and (8) we conclude that Q_2 must be a parallelogram. Similarly, it can also be concluded that Q_1 must be a parallelogram. Hence, the pattern is a $pgg^+{}_{2,2}$ variation of the Miura-ori presented in Fig. 6. For $\mu = \nu = 0$, the pattern is a Miura-ori.

From the above discussion, we conclude that a flat-foldable $pg_{2,2}$ derivative of the Miura-ori does not exist. The design generation process leading to this conclusion is illustrated in Fig. 7.

3.2. *The* M$^+$($pg_{2,2}$) *tessellation*

In the previous section, we proved that a flat-foldable $pg_{2,2}$ variation of the Miura-ori, M($pg_{2,2}$), does not exist. Starting from the alternative standard unit cell, S$^+$, illustrated in Fig. 1, this section discusses the $pg^+{}_{2,2}$ variation of the Miura-ori, M$^+$($pg_{2,2}$).

Theorem 3.2. *An* M$^+$($pg_{2,2}$) *tessellation is never flat-foldable.*

Proof. An M$^+$($pg_{2,2}$) unit cell is depicted in its original configuration, State 0, in Fig. 8a. Similar to the M$^+$($pg_{2,2}$) case, there are two distinct orbits of nodes associated with the unit cell, shown as A_0 and B_0. The details of the degrees of freedom for this case are similar to the $pg_{2,2}$ variation discussed earlier. As can be seen in Fig. 8b, we have perturbed the pattern using all the degrees of freedom that we introduced earlier to obtain a new configuration, State 1.

To investigate the application of the flat-foldability condition to the pattern at nodes A and B, we have illustrated a pair of consecutive quadrilaterals in the y-direction, from State 1 of the previous figure, in Fig. 9. For clarity, as we are dealing with a geometry problem, we ignore the naming scheme for symmetrically equivalent nodes associated with a unit cell. We have renamed the black nodes A_1 and B_1 as A and B, respectively, and the grey nodes A_1 and B_1 as A_g and B_g, respectively where g stands for glide-reflected. Nodes with index l represent the equivalent nodes on the left of each node A or B.

Line segments B_lA and A_lB_g have the same length, and the same acute angle (the absolute value of the angle is considered) with respect to the

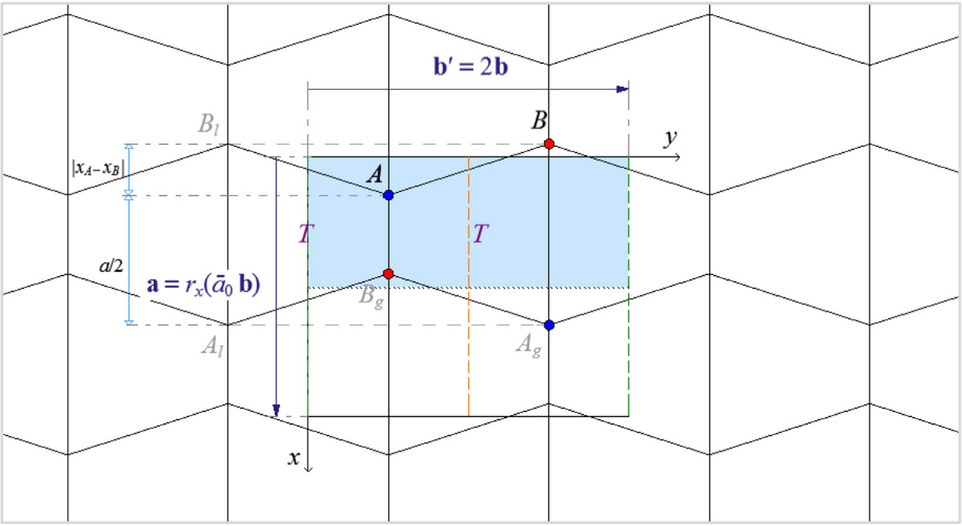

Fig. 12. A tessellation based on the previous figure; it is a non-legitimate variation of the Miura-ori with a (maximal) symmetry group *cmm*.

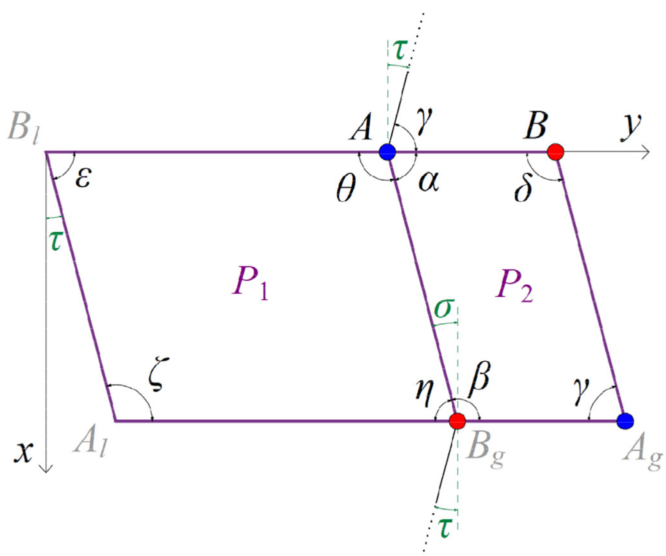

Fig. 13. The pair of consecutive quadrilaterals of Fig. 9 when $\mu = \nu = 0$.

y-axis, μ, as a result of the glide-reflection transformation. There is a similar relationship between line segments AB and B_gA_g, which intersect the y-axis at an angle ν. We assume that $\mu \neq 0$ and $\nu \neq 0$.

The two hatched triangles B_lAB and $A_lA_gB_g$ are congruent, as they have two congruent corresponding angles with a congruent included side. Therefore, the following relationship exists between their corresponding angles at nodes A and B_g

$$\zeta + \gamma = \varepsilon + \delta. \tag{9}$$

Applying the local flat-foldability condition, we can write the following equations in terms of the fold angles around nodes A and B

$$\alpha + \zeta = \pi, \tag{10}$$

$$\beta + \varepsilon = \pi. \tag{11}$$

Substituting the equivalents for ζ and ε from Eqs. (10) and (11) into Eq. (9) gives

$$\alpha + \delta = \beta + \gamma. \tag{12}$$

On the other hand, the internal angles of quadrilateral Q_2 must add up to 2π, i.e.

$$\alpha + \beta + \gamma + \delta = 2\pi. \tag{13}$$

From Eqs. (12) and (13) we can conclude

$$\alpha + \delta = \beta + \gamma = \pi. \tag{14}$$

This implies that AB_g is parallel to BA_g (and so to B_lA_l). In other words

$$\sigma = \tau. \tag{15}$$

The previous figure is repeated in Fig. 10 with some additional elements. A line is drawn from node A parallel to B_gA_l to intersect B_lA_l at a point M. The quadrilateral MA_lB_gA is a parallelogram, as it has two pairs of parallel opposite sides. Consequently, AM has the same length as B_gA_l, and as we already know that $B_gA_l = B_lA$, we conclude that triangle $T_1 = B_lMA$ is isosceles. As a result, we have

$$\varepsilon = \zeta. \tag{16}$$

In a similar way, and by drawing line segment AN parallel to B_gA_g from node A, we can conclude that

$$\delta = \gamma. \tag{17}$$

On the other hand, in parallelogram $B_lA_lA_gB$, the two adjacent angles at nodes B_l and A_l must add up to π, i.e., $(\varepsilon + \mu) + (\zeta + \mu) = \pi$; this gives

$$\varepsilon + \mu = \frac{\pi}{2}. \tag{18}$$

In a similar way, we can conclude

$$\nu + \delta = \frac{\pi}{2}. \tag{19}$$

Hence

$$\tau = 0. \tag{20}$$

Referring to Eq. (15), we conclude

$$\sigma = \tau = 0. \tag{21}$$

This means that parallelogram $B_lA_lA_gB$ must be a rectangle. It also implies that nodes A and B_g must be mirror nodes. Therefore, the following relationships must be satisfied

$$\zeta = \gamma \quad \text{and} \quad \varepsilon = \delta. \tag{22}$$

We know from elementary geometry that if in a triangle an altitude is also a bisector, the triangle is isosceles. Therefore

$$AB = AB_l = \frac{a}{2} + |x_A - x_B| \quad \text{and} \quad \mu = \nu = \arctan\left(|x_A - x_B|/b\right). \tag{23}$$

As a result, Q_1 and Q_2 are two congruent isosceles trapezoids, T, with a base equal to $\frac{a}{2} + |x_A - x_B|$ and a height (altitude) equal to b, as shown in Fig. 11.

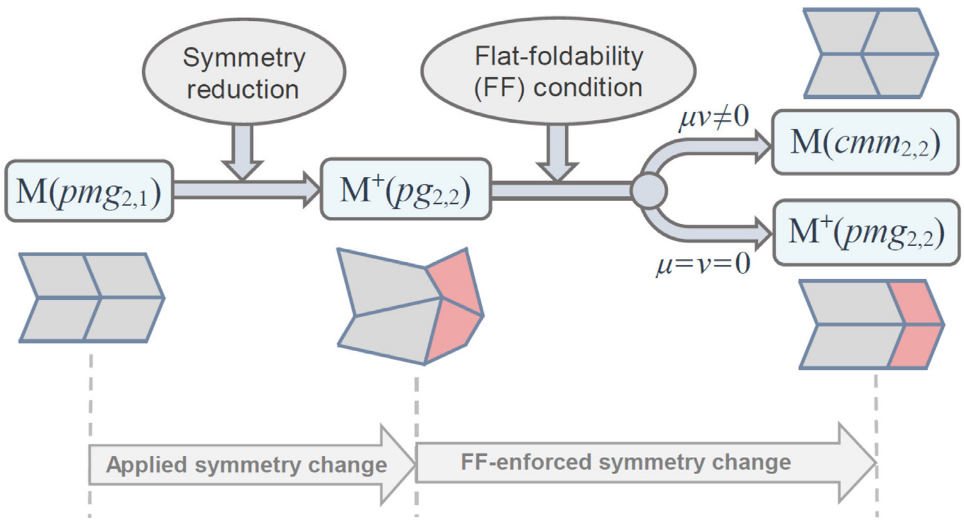

Fig. 14. Design generation process of the $pg^{+}{}_{2,2}$ derivative of the DDC surface.

A tessellation based on the previous figure is depicted in Fig. 12. It is a non-legitimate [49] variation of the Miura-ori, and its (maximal) symmetry group is *cmm*. In fact, it is a 90° rotated version of the bellow (or accordion) pattern (see, e.g. [51]).

Now we consider the case when $\mu = \nu = 0$. In this case, in order to have a flat-foldable pattern, both nodes A and B must be mirror nodes. Furthermore, as B_lB and A_lA_g are parallel, nodes A and B_g (and consequently B) must be geometrically congruent. As a result, there is only one acute angle in the pattern. In other words

$$\alpha = \gamma = \varepsilon = \eta. \tag{24}$$

Also we have

$$\tau = \sigma = \frac{\pi}{2} - \alpha. \tag{25}$$

Therefore, Q_1 and Q_2 are two different parallelograms, P_1 and P_2, sharing a side, as shown in Fig. 13. However, a tessellation based on P_1 and P_2 is not strictly *pg*, but it is $pmg^{+}{}_{2,2}$. If P_1 and P_2 are congruent, the resulted tessellation is the original Miura-ori. From the above discussion, we conclude that a flat-foldable $pg^{+}{}_{2,2}$ variation of the Miura-ori does not exist.

From the above discussion, we conclude that a flat-foldable $pg^{+}{}_{2,2}$ variation of the Miura-ori does not exist. The design generation process leading to this conclusion is illustrated in Fig. 14.

4. Conclusions

Exploring crystalline design variations of the developable double corrugation (DDC) surface or the Miura-ori, in this paper we studied the two minimal pg variations of this crease pattern in the longitudinal direction, namely $\mathrm{M}(pg_{2,2})$ and $\mathrm{M}^{+}(pg_{2,2})$. Both of these two tessellations are composed of two irregular quadrilaterals which tile the plane by glide reflections and translations, without having any rotational or reflectional symmetries. The main geometric difference between these two tessellations is that $\mathrm{M}(pg_{2,2})$ has a composition similar to a checkerboard, while $\mathrm{M}^{+}(pg_{2,2})$ consists of alternate strips of glide-reflected images of one tile.

By applying the local flat-foldability condition at the vertices of different orbits associated with each tessellation, we proved that such patterns are never flat-foldable, regardless of the geometric specifications of the two irregular quadrilaterals. This is because of the incompatibility between the crystalline structure of the patterns and the condition of local flat-foldability. In other words, we showed that no two irregular quadrilateral tiles can constitute a flat-foldable, developable double corrugation surface.

Declaration of Competing Interest

The authors declare that they have no known competing financial interests or personal relationships that could have appeared to influence the work reported in this paper.

CRediT authorship contribution statement

Pooya Sareh: Conceptualization, Methodology, Formal analysis, Visualization, Writing - original draft. **Yao Chen:** Investigation.

Acknowledgements

This research work has been partially supported by the National Natural Science Foundation of China (Grant numbers 51978150 and 51850410513).

References

[1] Miura K. Map Fold a La Miura Style, Its Physical Characteristics and Application to the Space Science. In: Takaki R, editor. Research of pattern formation. KTK Scientific Publishers; 1994. p. 77–90.
[2] Yoshimura, Y., On the mechanism of buckling of a circular cylindrical shell under axial compression, in NACA Technical Memorandum 1390. 1955, National Advisory Committee for Aeronautics; Washington, DC, United States.
[3] Rivas-Adrover E. A New Hybrid Type of Deployable Structure: origami-scissor Hinged. Journal of the International Association for Shell and Spatial Structures 2018;59(3):183–90.
[4] Yu H, Guo Z, Wang J. A method of calculating the degree of freedom of foldable plate rigid origami with adjacency matrix. Advances in Mechanical Engineering 2018;10(6):1687814018779696.
[5] Zhai Z, Wang Y, Jiang H. Origami-inspired, on-demand deployable and collapsible mechanical metamaterials with tunable stiffness. Proceedings of the National Academy of Sciences 2018;115(9):2032.
[6] Overvelde JTB, et al. A three-dimensional actuated origami-inspired transformable metamaterial with multiple degrees of freedom. Nat Commun 2016;7(1):10929.
[7] Zhang Q, et al. Origami and kirigami inspired self-folding for programming three--dimensional shape shifting of polymer sheets with light. Extreme Mech Lett 2017;11:111–20.
[8] Sareh P, et al. Rotorigami: a rotary origami protective system for robotic rotorcraft. Science Robotics 2018;3.
[9] Yoneda T, Matsumoto D, Wada H. Structure, design, and mechanics of a paper spring. Physical Review E 2019;100(1):013003.
[10] Zhao Z, et al. Origami by frontal photopolymerization. Sci Adv 2017;3(4):e1602326.
[11] Nojima T. Modelling of Folding Patterns in Flat Membranes and Cylinders by Origami. JSME International Journal Series C 2002;45(1):364–70.
[12] Sareh P. The least symmetric crystallographic derivative of the developable double corrugation surface: computational design using underlying conic and cubic curves. Mater Des 2019;183:108128.
[13] Demaine E. Folding and Unfolding. UWSpace 2001.
[14] Glugla DJ, et al. Rigid Origami via Optical Programming and Deferred Self-Folding of a Two-Stage Photopolymer. ACS Appl Mater Interfaces 2016;8(43):29658–67.

[15] Zhang Z, et al. A rigid thick Miura-Ori structure driven by bistable carbon fibre-reinforced polymer cylindrical shell. Compos Sci Technol 2018;167:411–20.
[16] Liu J, et al. Fabrication, dynamic properties and multi-objective optimization of a metal origami tube with Miura sheets. Thin-Walled Structures 2019;144:106352.
[17] Zingoni A. Group-theoretic applications in solid and structural mechanics: a review. Computational structures technology. GBR: Civil-Comp press; 2002. p. 283–317.
[18] Bai Y, et al. Exploiting group symmetry in truss topology optimization. Optimization and Engineering 2009;10(3):331–49.
[19] Chen Y, et al. An Integrated Geometric-Graph-Theoretic Approach to Representing Origami Structures and Their Corresponding Truss Frameworks. Journal of Mechanical Design 2019;141(9):091402–091402-8.
[20] Jacobsen AJ, Barvosa-Carter W, Nutt S. Micro-scale truss structures with three–fold and six-fold symmetry formed from self-propagating polymer waveguides. Acta Mater 2008;56(11):2540–8.
[21] Chen Y, et al. Nodal flexibility and kinematic indeterminacy analyses of symmetric tensegrity structures using orbits of nodes. International Journal of Mechanical Sciences 2019;155:41–9.
[22] Chen Y, Feng J, Sun Q. Lower-order symmetric mechanism modes and bifurcation behavior of deployable bar structures with cyclic symmetry. Int J Solids Struct 2018;139:1–14.
[23] Chen Y, et al. A computational method for automated detection of engineering structures with cyclic symmetries. Comput Struct 2017;191:153–64.
[24] Chen Y, Sareh P, Feng J. Effective insights into the geometric stability of symmetric skeletal structures under symmetric variations. Int J Solids Struct 2015;69:277–90.
[25] Zingoni A, Pavlovic MN, Zlokovic GM. A symmetry-adapted flexibility approach for multi-storey space frames. Part 1: general outline and symmetry-adapted redundants.. Structural Engineering Review 1995;2(7):107–19.
[26] Chen Y, Yan J, Feng J, Sareh P. Particle Swarm Optimization-Based Metaheuristic Design Generation of Non-Trivial Flat-Foldable Origami Tessellations With Degree-4 Vertices. J. Mech. Des. 2020:1–25 MD-19-1839.
[27] Chen Y, Yan J, Feng J, Sareh P. Feasible prestress modes for cable-strut structures with multiple self-stress states using particle swarm optimization. Journal of Computing in Civil Engineering 2020;34(3).
[28] Chen Y, Yan J, Feng J, Sareh P. A hybrid symmetry–PSO approach to finding the self--equilibrium configurations of prestressable pin-jointed assemblies. Acta Mechanica 2020(4).
[29] Connelly R, Back A. Mathematics and tensegrity: group and representation theory make it possible to form a complete catalogue of“ strut-cable” constructions with prescribed symmetries. Am. Sci. 1998;86(2):142–51.
[30] Connelly R, Terrell M. Globally rigid symmetric tensegrities. Structural Topology 1995 núm 21 1995.
[31] Masic M, Skelton RE, Gill PE. Algebraic tensegrity form-finding. Int J Solids Struct 2005;42(16–17):4833–58.
[32] Chen Y, et al. Feasible Prestress Modes for Cable-Strut Structures with Multiple Self--Stress States Using Particle Swarm Optimization. Journal of Computing in Civil Engineering 2020;34(3):04020003.
[33] Zingoni A. On the symmetries and vibration modes of layered space grids. Engineering Structures 2005;27(4):629–38.
[34] Zingoni A. Symmetry recognition in group-theoretic computational schemes for complex structural systems. Comput Struct 2012;94:34–44.
[35] Sibley TQ. Thinking geometrically: a survey of geometries, 26. The Mathematical Association of America; 2015.
[36] MacLaren MD, Marsaglia G. Uniform random number generators. Journal of the ACM (JACM) 1965;12(1):83–9.
[37] Oberkampf WL. Domain mappings for the numerical solution of partial differential equations. Int J Numer Methods Eng 1976;10(1):211–23.
[38] Forney GD. Geometrically uniform codes. IEEE Transactions on Information Theory 1991;37(5):1241–60.
[39] Uspenskij V. The Urysohn universal metric space is homeomorphic to a Hilbert space. Topol Appl 2004;139(1–3):145–9.
[40] Klein F. A comparative review of recent researches in geometry. Bulletin of the American Mathematical Society 1893;2(10):215–49.
[41] Coxeter HSM, Greitzer SL. Geometry revisited, 19. Maa; 1967.
[42] Schwarzenberger RLE. The 17 plane symmetry groups. Mathematical Gazette 1974;58:123–31.
[43] Schattschneider D. The plane symmetry groups: their recognition and notation. The American Mathematical Monthly 1978;85(6):439–50.
[44] Conway JH, Huson DH. The Orbifold Notation for Two-Dimensional Groups. Struct Chem 2002;13(3):247–57.
[45] Coxeter HSM, Moser WOJ. Generators and relations for discrete groups, 14. Springer Science & Business Media; 2013.
[46] Macbeath AM. The classification of non-euclidean plane crystallographic groups. Canadian Journal of Mathematics 1967;19:1192–205.
[47] Hahn T. International tables for crystallography, volume A: space-group symmetry. USA: Springer; 2005.
[48] Sareh P. Symmetric Descendants of the Miura-ori. PhD Dissertation. Engineering Department, University of Cambridge, UK 2014.
[49] Sareh P, Guest SD. A Framework for the Symmetric Generalisation of the Miura-ori. International Journal of Space Structures, Special Issue on Folds and Structures 2015.
[50] Sareh P, Guest SD. Designing symmetric derivatives of the Miura-ori. Advances in Architectural Geometry 2014. Springer International Publishing; 2014. p. 233–41.
[51] Jackson P. Folding techniques for designers-from sheet to form. Mac Win Pa: Laurence King Publishing; 2011. ISBN 978-1856697217.
[52] Barreto PT. Lines meeting on a surface: the “MARS” paperfolding. in origami science & art: proceedings of the second international meeting of origami science and scientific origami. Japan: Otsu; 1997.
[53] Sareh P, Guest SD. Design of isomorphic symmetric descendants of the Miura-ori. Smart Materials and Structures 2015;24(8):085001.
[54] Sareh P, Guest SD. Design of non-isomorphic symmetric descendants of the Miura-ori. Smart Materials and Structures 2015;24(8):085002.